Journal of Ceramic Processing Research. Vol. 21, No. 1, pp. 119~122 (2020)
(Received 14 November 2019, Received in revised form 15 December 2019, Accepted 24 December 2019)
https://doi.org/10.36410/jcpr.2020.21.1.119

J O U R N A L O F
Ceramic Processing Research

Synthesis of three-dimensional cactus-shaped SnO_2 crystals via thermal evaporation of Sn

Min-Sung Kim*
Department of Information & Communications Engineering, Tongmyong University, Busan 48520, Korea

SnO_2 crystals were fabricated by thermal evaporation of Sn powder at 900°C in an oxygen atmosphere without any catalyst. The growth time was varied in a range of 1 ~ 3 h in order to investigate the morphological change during growth of the crystals. Scanning electron microscopy, X-ray diffractometry, energy dispersive X-ray spectroscopy, and cathodoluminescence spectroscopy were used to characterize the morphologies, crystal structures, and luminescence properties of the SnO_2 crystals. X-ray diffraction analysis showed that the SnO_2 crystals had a rutile crystallographic structure. When the growth time was 1 h, SnO_2 microrods with a rough surface were observed. With an increase of the growth time to 2 h, many nanowires on the SnO_2 microrods such that microrod-nanowire assembly had a cactus-like appearance. When the growth time was further increased to 3 h, micro/nanowires were observed. A strong visible emission peak centered at about 480 nm was observed in the room temperature cathodoluminescence spectra of all the samples.

Keywords: Tin powder, Thermal evaporation, Tin oxide micro-rods, Cactus shape.

Introduction

Metal-oxide micro/nanocrystals recently have attracted attention due to their novel properties and potential applications in electronics and optoelectronics. Micro/nanocrystals of functional metal oxides have been synthesized because they lend the possibility of fabricating smart devices by exploiting their novel electrical, optical, and magnetic properties. Among functional metal oxides, SnO_2 with a wide band gap of 3.6 eV is one of the most important metal oxides with many applications. It has been widely employed in various fields of solar cells, light emitting diodes, transparent electrodes, transistors, photovoltaic cells, lithium ion battery electrodes, and gas sensors.

In particular, SnO_2 is an outstanding material for gas sensors due to its advantages including high sensitivity, fast response and recovery time, chemical and thermal stability, and high mechanical strength. Thus, SnO_2 is widely used as gas sensing material to detect extremely hazardous gases. The sensing mechanism of SnO_2 is based on the change in the conductivity which is caused by the reaction between the oxygen and the detected gas on the surface of the SnO_2 material. Hence, the surface area has a strong impact on the sensing performance. The sensing performance is improved with an increase in the surface area of sensing material. In general, micro/nanocrystals have large surface area, which results in the enhancement of the sensing performance [1-5]. Accordingly, consideration effort has been devoted to the synthesis of SnO_2 micro/nanocrystals.

So far, diverse morphologies of SnO_2 micro/nanocrystals such as wires [6], belts [7], rods [8], and tubes [9] have been synthesized. Especially, a three-dimensional (3D) hierarchical morphology such as flower-like and dendritic shapes is thought to be most effective for improving the sensing performance of gas sensors due to the high surface area relative to volume [10]. In addition, 3D morphology is favorable for the diffusion of gas molecules, which is important for improving the sensitivity and response time of gas sensors. Thus, the facile synthesis of SnO_2 crystals with a 3D morphology is of considerable interest.

SnO_2 micro/nanocrystals with a 3D morphology have been mainly synthesized using wet chemical methods including hydrothermal and sol-gel methods [11-15]. The wet chemical processes are carried out at relatively low temperatures. The drawback of the low-temperature processes is the poor crystallinity of micro/nanocrystals. Therefore, dry process methods have received increasing attention in synthesizing 3D SnO_2 micro/nanocrystals. The dry methods include thermal evaporation, chemical vapor deposition, and pulsed laser deposition. Among them, thermal evaporation is a relatively simple and low cost technique. There are few reports on the synthesis of 3D SnO_2 micro/nanocrystals using thermal evaporation [16, 17]. In the reports, the 3D SnO_2 micro/nanocrystals were grown via vapor-liquid-solid (VLS) mechanism. Metal catalysts are essential in the VLS mechanism. But the catalysts can create contamination in the micro/

*Corresponding author:
Tel : +82-51-629-1148
Fax: +82-51-629-1148
E-mail: minsung@tu.ac.kr

nanocrystals. Thus, it is worthwhile to develop a catalyst-free thermal evaporation process for synthesizing 3D SnO_2 micro/nanocrystals.

In this paper, the facile synthesis of 3D cacti-like SnO_2 crystals via thermal evaporation of Sn powder without using catalyst is reported.

Experimental

Sn powder with a purity of 99.99% was used as the source material. The alumina crucibles with the Sn powder were placed in the middle of a horizontal quartz tube furnace. The quartz tube was evacuated to a pressure of 1×10^{-1} Torr by using a mechanical pump. Then oxygen was introduced into the quartz tube until the pressure reached 100 Torr. The pressure was maintained at 100 Torr throughout the experiment. The temperature was set to 900 °C and the growth time was varied in a range of 1 ~ 3 h to investigate the effect of growth duration on the morphology of the products. The furnace was subsequently cooled to room temperature. The products in the crucibles were collected for characterization.

X-ray diffraction (XRD) patterns were obtained to investigate the crystalline structure of the as-synthesized products. Field emission scanning electron microscopy (FESEM) was used to investigate the crystalline structure of the as-synthesized products. An energy dispersive X-ray (EDX) spectroscope was employed to study the components of the products. The cathodoluminescence (CL) measurement was carried out at room temperature.

Results and Discussion

Fig. 1 shows the XRD spectra of the products synthesized by thermal evaporation of Sn powder at 900 °C in an O_2 ambient for 1 h, 2 h, and 3 h, respectively. XRD spectra reveal similar XRD peak patterns for all the products. The diffraction peaks are identical to the tetragonal rutile structure of SnO_2 with lattice constants of $a = b = 0.473$ nm and $c = 0.318$ nm, indicating that all the products are SnO_2 with a rutile structure. No peaks were detected for other crystalline phase of impurities.

Fig. 2 shows the EDX spectra of the products synthesized by thermal evaporation of Sn powder at 900 °C in an O_2 ambient for 1 h, 2 h, and 3 h, respectively. Only Sn and O are detected in the spectra, which confirms that the products are high purity SnO_2.

Fig. 3 shows SEM images of the SnO_2 crystals synthesized by thermal evaporation of Sn powder at 900 °C in an O_2 ambient for 1 h, 2 h, and 3 h, respectively. When the growth time was 1 h, SnO_2 microrods with a rough surface were observed. The SnO_2 microrods have an average diameter of 4 μm and lengths of several tens of micrometers. SnO_2 micro/nanowires with a rough surface have been observed in products synthesized

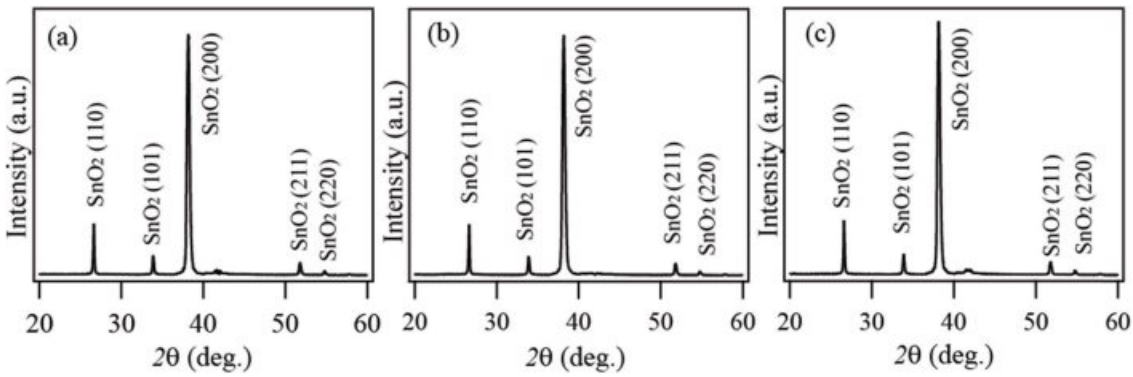

Fig. 1. XRD spectra of the products synthesized at 900°C for (a) 1 h, (b) 2 h and (c) 3 h, respectively.

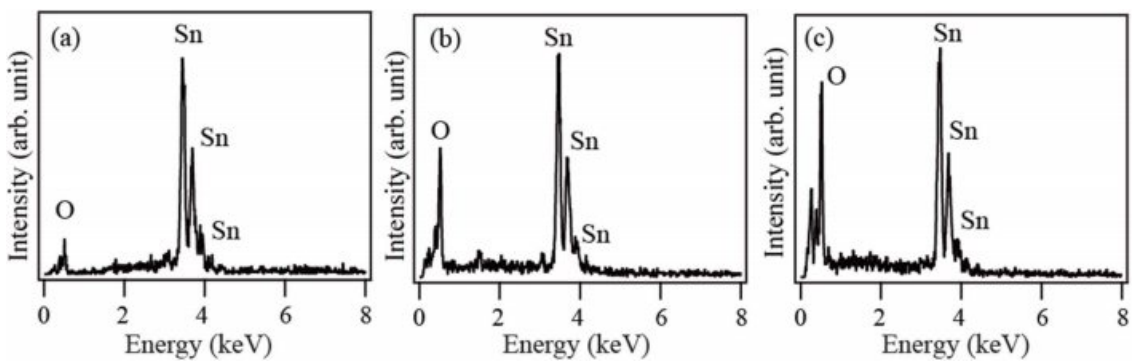

Fig. 2. EDX spectra of the products synthesized at 900°C for (a) 1 h, (b) 2 h and (c) 3 h, respectively.

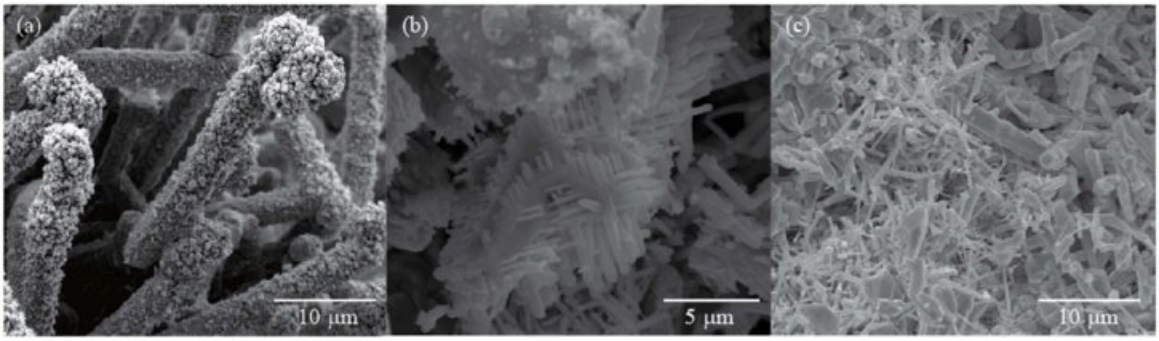

Fig. 3. SEM images of the products synthesized at 900°C for (a) 1 h, (b) 2 h and (c) 3 h, respectively.

through thermal evaporation of Sn under a vacuum condition [18]. Upon increasing the growth time to 2 h, the SEM image exhibits SnO_2 microrods on which nanowires with high density are grown. The SnO_2 microrod consists of a main micro-sized stem and numerous nanowires on the stem, which resembles a cactus-like structure. The nanowires are grown on the rough surface of the main stem. The main stems are 0.25 ~ 1 μm in diameter and 7 ~ 15 μm in length, respectively. The diameter and the length of the nanowires are 50 ~ 250 nm and 0.5 ~ 1.5 μm, respectively. Secondary branched nanowires as well as primary branched nanowires are observed in the SEM images. The branched nanowires have uniform diameter along the growth direction, which indicates that the growth conditions remained constant during the growth. The secondary branched nanowires were grown in a perfectly perpendicular direction to the side of the main stem.

The growth mechanism of the cactus-like SnO_2 microrods with branched nanowires is posited as follows. Initially, Sn powder is vaporized into Sn vapor. The Sn vapor reacts with the oxygen in the atmosphere to form SnO_2 nuclei. The nuclei grow along the preferential direction, leading to the formation of main stems. The size of the main stems increases with the growth time. Secondary nucleation and growth occur on the main stems, which are sufficiently large to promote secondary nucleation on their surfaces. The secondary nucleation leads to the growth of primary branched nanowires on the main stems. The same growth process is repeated on the primary branched nanowires, resulting in the formation of secondary branched nanowires. The rough surface of the main stems would favor secondary nucleation. On the other hand, in the present experiment, the growth of main stems and branched nanowires is considered to proceed via a vapor-solid (VS) mechanism because no catalysts were used and no catalyst droplets were found at the tips of the nanowires. There are two growth mechanisms in the growth of the one-dimensional nanowires and nanorods. One is vapor-solid (VS) mechanism and the other is vapor-liquid-solid (VLS) mechanism. In the VLS mechanism, metal catalyst is required to direct the crystal growth on to specific orientation. The metal catalyst forms liquid droplets and adsorbs vapor components at the growth temperature. When the liquid droplets become supersaturated with the absorbed components, the components start to precipitate and continued precipitation results in the growth of nanowires. Therefore, catalyst particles are typically observed at the tips of nanowires grown via VLS mechanism [19, 20]. In this work, no catalyst particles were observed at the tips of the branched nanowires, indicating that the nanowires were grown via VS mechanism.

After growth time of 3 h, SnO_2 microrods with

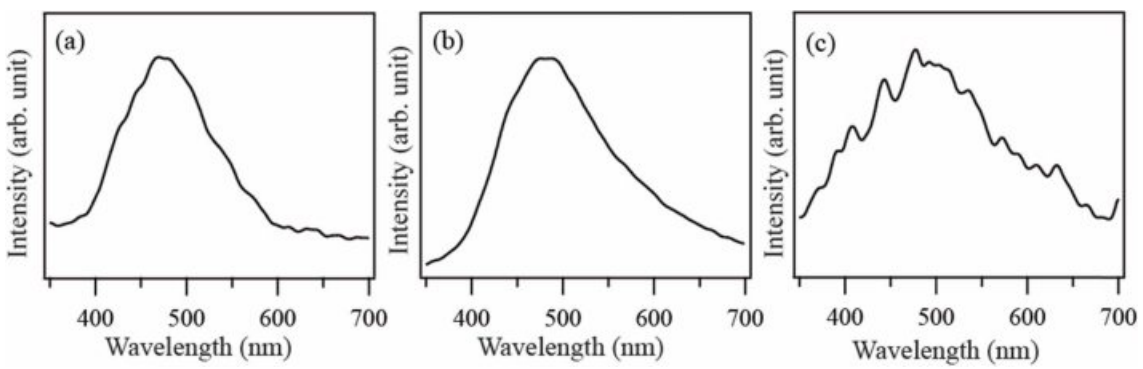

Fig. 4. Room temperature CL spectra of the products synthesized at 900°C for (a) 1 h, (b) 2 h and (c) 3 h, respectively.

branched nanowires were not observed and micro/nanowires were found. It is known that SnO_2 is an oxide that becomes unstable above 500 °C [21]. Thus, in the present work, the SnO_2 microrods would decompose into Sn and oxygen because of prolonged growth time and then Sn vapor would react with oxygen to form SnO_2 nanowires.

Figs. 4(a), (b), and (c) show the CL spectra of the SnO_2 crystals synthesized by thermal evaporation of Sn powder at 900 °C in an O_2 ambient for 1 h, 2 h, and 3 h, respectively. A broad visible emission with a maximum at 480 nm is dominantly observed in the CL spectra. The broad visible emission has been observed from SnO_2 crystals at room temperature [22, 23]. The visible luminescence is known to be associated with oxygen vacancies. Luo et al reported that the emission peak at 480 nm also originated from surface oxygen vacancies [24]. Because SnO_2 is an n-type semiconductor, the presence of oxygen vacancies is related to the n-type semiconducting property. Accordingly, it is suggested that the visible emission observed in the present experiment can be attributed to oxygen-related defects.

Conclusion

SnO_2 micro/nanocrystals with a tetragonal rutile structure could be formed via thermal evaporation of Sn powder in oxygen ambient at 100 Torr. The morphology of SnO_2 micro/nanocrystals was significantly affected by an increase in growth time. As growth time increased, the morphology of the SnO_2 micro/nanocrystals changed from microrods to cactus-like microrods on which numerous nanowires were grown. The cactus-like microrods consisted of main stems and many branched nanowires. Secondary branched nanowires as well as primary branched nanowires were observed on the microrods. It is considered that the 3D cactus-like hierarchical SnO_2 crystals were grown via VS growth. In the room temperature CL spectra, a strong visible emission at 480 nm was observed, and this might be attributable to oxygen vacancies. The unique 3D cactus-like SnO_2 crystals have high accessible surface area and considerable inter-nanowire space, which can provide more active sites. Thus the cactus-like crystals can be used as a potential material for highly efficient gas sensors, catalysts, dye-sensitized solar cells, and Li-ion batteries.

Acknowledgement

This Research was supported by the Tongmyong University Research Grants 2019.

References

1. S. Supothina, M. Suwan, and A. Wisitsoraat, J. Ceram. Process. Res. 14 (2013) 226-229.
2. H. Yu, T. Yang, Z. Wang, Z. Li, B. Xiao, Q. Zhao, and M. Zhang, J. Alloy. Compd. 724 (2017) 121-129.
3. R. Zhao, Z. Wang, Y. Yang, X. Xing, T. Zou, Z. Wang, and Y. Wang, J. Phys. Chem. Solids 120 (2018) 173-182.
4. X. Lian, Y. Li, J. Zhu, Y. Zou, X. Liu, D. An, and Q. Wang, Curr. Appl. Phys. 19 (2019) 849-855.
5. T. Li, W. Zeng, H. Long, and Z. Wang, Sens. Actuat. B-Chem. 231 (2016) 120-128.
6. J.M. Jeong, Y.J. Kwon, H.Y. Cho, H.G. Na, and H.W. Kim, J. Ceram. Process. Res. 15 (2014) 428-432.
7. S.H. Sun, G.W. Meng, Y.W. Wang, T. Gao, M.G. Zhang, Y.T. Tian, X.S. Peng, and L.D. Zhang, Appl. Phys. A. 76 (2003) 287-289.
8. H.W. Kim, J.W. Lee, S.H. Shim, and C. Lee, J. Korean Phys. Soc. 51 (2007) 198-203.
9. W. Jin, Z. Tian, L. Lin, D. Jiatao, Z. Gang, Z. Pei, J. Yong, J. Zhifeng, and S. Xiaosong, Mater. Lett. 180 (2016) 38-41.
10. H. Wang, and A.L. Rogach, Chem. Mater. 26 (2014) 123-133.
11. J.R. Hunag, K. Yu, C.P. Gu, M.H. Zhai, Y.J. Wu, M. Yang, and J.H. Liu, Sens. Actuat. B-Chem. 147[2] (2010) 467-474.
12. H. Wang, Q.Q. Liang, W.J. Wang, Y.R. An, J.H. Li, and L. Guio, Cryst. Growth Des. 11 (2011) 2942-2947.
13. R. Yang, Y.G. Gu, Y.Q. Li, J. Zheng, and X.G. Li, Acta Mater. 58 (2010) 866-874.
14. Y.L. Wang, M. Guo, M. Zhang, and X.D. Wang, Scripta Mater. 61 (2009) 234-236.
15. Q, Wang, L.S. Zhang, J.F. Wu, W.D. Wang, W.G. Song, and W. Wang, J. Phys. Chem. C 114 (2010) 22671-22676.
16. Z. Guo, X. Chen, W.H. Xu, J. Li, G.M. Yang, M.Q. Li, J.H. Liu, and X.J. Huang, Mater. Today 14 (2011) 42-49.
17. S.H. Mohamed, J. Alloy. Compd. 510 (2012) 119-124.
18. N.M. Shaalan, T. Yamazaki, and T. Kikuta, Sens. Actuat. B-Chem. 153[1] (2011) 11-16.
19. W.I. Park, J. Ceram. Process. Res.9 (2008) 666-671.
20. R.S. Wagner, and W.C. Ellis, Appl. Phys. Lett. 4 (1964) 89-90.
21. D. Zhang, X. Li, F. Wan, C.J. Thong, M.A. Rindfleisch, M.J. Tomsic, M.D. Sumption, and E.W. Collings, Mater. Sci. Eng. 279 (2017) 012025.
22. S.H. Luo, Q. Wan, W.L. Liu, M. Zhang, Z.T. Song, C.L. Lin, and P.K. Chu, Prog. Solid State Chem. 33 (2005) 287-292.
23. S. Luo, J. Fan, W. Liu, M. Zhang, Z. Song, C. Lin, X. Wu, and Paul K. Chu, Nanotechnology 17 (2006) 1695-1699.
24. S. Luo, P.K. Chu, W. Liu, M. Zhang, and C. Lin, Appl. Phys. Lett. 88 (2006) 183112.